Published in *Bioorg. Med. Chem. Lett.* **2015**, *25*, 642-648

http://dx.doi.org/10.1016/j.bmcl.2014.12.001

Potent and selective MAO–B inhibitory activity: amino–versus nitro–3–arylcoumarin derivatives

Maria João Matos,[a,*] Fernanda Rodríguez–Enríquez,[b] Santiago Vilar,[a,c] Lourdes Santana,[a] Eugenio Uriarte,[a] George Hripcsak,[c] Martín Estrada,[d] María Isabel Rodríguez–Franco[d] and Dolores Viña[b]

[a] *Departamento de Química Orgánica, Facultad de Farmacia, Universidad de Santiago de Compostela, 15782 Santiago de Compostela, Spain*

[b] *Departamento de Farmacología, CIMUS, Universidad de Santiago de Compostela, 15782 Santiago de Compostela, Spain*

[c] *Department of Biomedical Informatics, Columbia University Medical Center, 10032 New York, USA*

[d] *Instituto de Química Médica, Consejo Superior de Investigaciones Científicas (IQM–CSIC), C/ Juan de la Cierva 3, 28006 Madrid, Spain*

** Fax: +34 981 544912; Tel: +34 881 814936; E–mail: mariacmatos@gmail.com*

ABSTRACT

In this study we synthesized and evaluated a new series of amino and nitro 3–arylcoumarins as hMAO–A and hMAO–B inhibitors. Compounds 2, 3, 5 and 6 presented a better activity and selectivity profile against the hMAO–B isoform (IC_{50} values between 2 and 6 nM) than selegiline. In general, the amino derivatives (4–6) proved to be more selective against MAO–B than the nitro derivatives (1–3). Additionally, a theoretical study of some physicochemical properties, PAMPA and reversibility assays for the most potent derivative, and molecular docking simulations were carried out to further explain the pharmacological results, and to identify the hypothetical binding mode for the compounds inside the hMAO–B.

Neurodegeneration is a large class of chronic and progressive nervous system biochemical processes based on constitutional neuronal degeneration. The wrong regulation of these processes leads to different neurodegenerative diseases (ND), such as **Alzheimer's disease (AD), Parkinson's disease (PD),** amyotrophic lateral sclerosis, and Huntington disease.[1] Among them, AD and PD are the most prevalent. The etiology of these diseases is not completely known, but several risk factors have been identified, including environmental factors, genetics, and age.[1,2] Several research hypotheses exist regarding the pathogenesis, including different mechanisms that may be involved in the development of the disease, such as oxidative stress, inflammation, excitotoxicity, mitochondrial dysfunction and proteolytic stress.[2] These pathologies severely influence the life quality of the elderly.[3] Therefore, studies in the area are continuously improving.

PD, the second most important ND, is characterized by loss of dopaminergic neurons in the nigro–striatal pathway. These neurons extend from the zona compacta of the substantia nigra (SNC) to the striatum.[3] The symptoms of PD, resting tremor, rigidity and bradykinesia, appear when about 80% of dopaminergic neurons have been destroyed.[4] **In the 50's,** dopamine (DA) was described as a neurotransmitter, which showed low levels in the basal ganglia in animal models of Parkinsonism. After the success of a placebo–controlled trial, levodopa (LD) became an essential drug for the treatment of PD.[5] Even today the standard treatment of PD is the combination of LD with inhibitors of peripheral dopa decarboxylase (DDC), to avoid the formation of DA in the periphery.[5] LD is also associated to inhibitors of the enzyme catechol–*O*–methyltransferase (COMT) and prevents the formation of 3–*O*–methyldopa (3–OMD).[6] Among other drugs that can be used to treat PD, selective inhibitors of monoamine oxidase B (MAO–B) play an important role.[7,8] MAO–B metabolizes approximately 80% of the DA in the SNC, without affecting the serotonine or noradrenaline metabolism. MAO is a flavin–containing enzyme bound to the mitochondrial outer membrane of neuronal, glial, and other cells, which is responsible for the oxidative deamination of endogenous monoamine neurotransmitters, trace amines, and a number of amine xenobiotics.[9] This enzyme exists in two distinct enzymatic isoforms, namely MAO–A and MAO–B encoded by different genes and distributed in diverse tissues.[10] Increased activity of MAO–A and MAO–B is associated with loss of endogenous and exogenous monoamine amounts.

An increase in MAO-B activity is also associated with gliosis, which can result in high levels of hydrogen peroxide and oxidative free radicals. Evidence exists that as aging progresses activity of MAO-B in the brain increases, but not so for MAO-A.[8] The largest increases are in the basal ganglia and thalamus, followed by the frontal cortex and, to a lesser extent, cerebellum and parietal and temporal cortices.[11]

Some studies have demonstrated the preliminary dominance of coumarin compounds in the treatment of AD and PD for improving the elderly's life quality. Coumarins represent an important family of naturally occurring[12] and/or synthetic oxygen-containing heterocycles, bearing a typical benzopyrone framework.[13] Therefore, coumarinic compounds are a class of lactones structurally constructed by a benzene ring fused α-pyrone ring, and essentially possess π–π conjugated system with rich electron and good charge-transport properties.[14] The simplicity and versatility of the coumarin scaffold make it an interesting starting-point for a wide range of biological applications.[15,16] Moreover, a significant number of coumarin compounds are being actively developed as medicinal candidates or drugs with strong pharmacological activity, low toxicity and fewer side-effects, lower drug resistance, high bioavailability, broad spectrum and better curative effects, etc.[17] Several efforts have been made mainly in developing coumarin-based anticoagulant, antioxidant, antimicrobial (antiviral, antifungal and antiparasitic), anticancer, antidiabetic, analgesic, anti-neurodegenerative and anti-inflammatory agents.[18-23] Nowadays, some coumarins proved to be enzymatic inhibitory agents [MAO inhibitors, acetylcholinesterase (AChE) inhibitors and butyrylcholinesterase (BuChE) inhibitors] with potential in ND.[24-27] These studies represent an important tendency in the coumarin's chemistry and biological evaluation.[28,29]

Early literature reported that electron delocalization and polarizability as well as hydrophobicity were crucial physical factors for MAO inhibitors.[30] The fused coumarins with large conjugated system demonstrated better MAO-B inhibitory activity than the reference compounds. Therefore, fused coumarins are also worthy of further investigation as potential MAO-B inhibitors.[31] Some interesting structure-activity relationships were concluded from these studies. Literature has also reported that some compounds with acyl or benzyloxy substituted group linked to C-3 or C-7 position at the coumarin ring possess the ability to improve inhibitory activity and selectivity towards MAO-B.[32]

In addition, previous work has been done by our group modulating the positions 3 and 6 of the coumarin ring with different substituents.[33,34] Our research group has reported, in several studies, the importance of the MAO inhibitory activity of different substituents on the phenyl ring at position 3 of the 3-arylcoumarins in the PD.[35-37] Comparative studies suggested that substitutions (methoxy and methyl groups, and bromine atoms) at *meta* and *para* positions of the 3-aryl group played an important role in exerting the biological activity and selectivity against MAO-B. Several compounds proved to be better than the reference compounds selegiline and rasagiline. Other substitutions on this moiety that can modulate also the activity and selectivity against MAO enzymes were also studied by our group.[38] Different substitutions of the coumarin nucleus at 3-position result in different activity and selectivity to MAO-B, also those derivatives with different heterocyclic rings in this position possess potency and selectivity towards MAO-B.[39]

Therefore, almost all the studied derivatives might be considered as potential lead compounds for treating PD. Taking into account this previous results, the introduction of nitro and amino groups in the 3-aryl ring of 3-arylcoumarins seems to be of high interest. A comparison between both substituents in different positions was performed in this new study. Docking calculations were an important tool to support and better understand the results, and also to the rational design of new derivatives.

6-Methyl-3-nitrophenylcoumarins 1-3 were synthesized starting from the commercially available 5-methylsalicylaldehyde and the respectively substituted 3-nitrophenylacetic acids by a modified Perkin reaction, in good yields (70-80%). The amino-derivatives 4-6 were obtained, in very good yield (92-97%), from 1-3, respectively, in a palladium/carbon catalyzed reaction.[40,41,42]

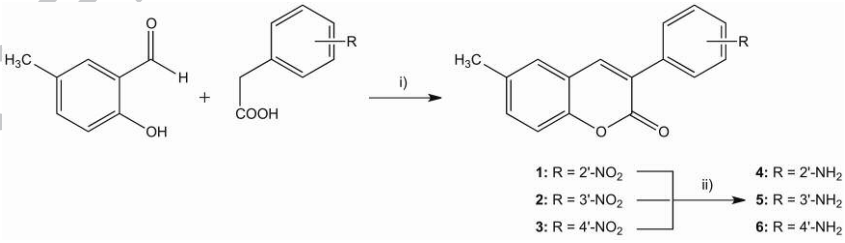

Scheme 1. Synthesis of 3-arylcoumarins. *Reagents and conditions*: (i) NaH, Ac_2O, r.t., 20 h; (i) H_2, Pd/C, ethanol, r.t., 3 h.

The biological evaluation of the test drugs on hMAO activity was investigated by measuring their effects on the production of H_2O_2 from *p*-tyramine (a common substrate for hMAO-A and hMAO-B), using the Amplex® Red MAO assay kit and microsomal MAO isoforms prepared from insect cells (BTI-TN-5B1-4) infected with recombinant baculovirus containing cDNA inserts for hMAO-A or hMAO-B.[43,44] New compounds and reference inhibitors were unable to react directly with the Amplex® Red reagent, which indicates that these drugs do not interfere with the measurements. On the other hand, in the experiments and under the experimental conditions, hMAO-A displayed a Michaelis constant (K_m) equal to 457.17 ± 38.62 μM and a maximum reaction velocity (V_{max}) in the control group of 185.67 ± 12.06 (nmol *p*-tyramine/min)/mg protein, whereas hMAO-B showed a K_m of 220.33 ± 32.80 μM and V_{max} of 24.32 ± 1.97 (nmol *p*-tyramine/min)/mg protein (n = 5). Most tested compounds concentration-dependently inhibited this enzymatic control activity (Table 1).

Table 1. hMAO-A and hMAO-B in vitro inhibitory activity of the synthesized derivatives 1-6 and reference compounds.[a]

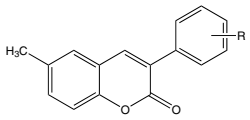

Comp.	R	IC_{50} hMAO-A (nM)	IC_{50} hMAO-B (nM)	S. I.[b]
1	**2'**-NO_2	*	$5.52\times10^3 \pm 0.30\times10^3$	> 18[d]
2	**3'**-NO_2	*	6.00 ± 0.40	> 16,667[d]
3	**4'**-NO_2	$4.18\times10^3 \pm 0.28\times10^3$[c]	2.10 ± 0.10	2,090
4	**2'**-NH_2	*	$2.17\times10^3 \pm 0.15\times10^3$	> 46[d]
5	**3'**-NH_2	*	2.20 ± 0.13	> 50,000[d]
6	**4'**-NH_2	*	4.10 ± 0.27	> 25,000[d]
Selegiline	–	$67.25\times10^3 \pm 1.02\times10^3$[c]	19.60 ± 0.86	3,431
Moclobemide	–	361.38 ± 19.30	*	**0.0036**[d]

[a] Each IC_{50} value is the mean ± S.E.M. from five experiments (n = 5). [b] Selectivity index: MAO-B selectivity ratios [IC_{50} (MAO-A)]/[IC_{50} (MAO-B)] for inhibitory effects of both new compounds and reference inhibitors. [c] $p < 0.01$ regarding the corresponding IC_{50} obtained against MAO-B as determined by ANOVA/Dunnett's. [d] Values obtained under the assumption that the corresponding IC_{50} against either MAO-A or MAO-B is greater than 100 μM. * Inactive at 100 μM (highest concentration tested).

A basic condition of any compound to act on neurodegenerative processes is to penetrate into the brain, that is, to be able to cross the blood–brain barrier (BBB). To examine the capability of our compounds to pass this barrier, we selected compound 3, the most active, with a nitro group in the phenyl at 3-position, and used a parallel artificial membrane model.[27] This is a fairly easy and successful method to predict the passive central nervous system (CNS) permeation, which had been previously optimized in order to be applied to investigational compounds with limited aqueous solubility.[45–47] The permeability of compounds 3 through a lipid extract of porcine brain were determined using a mixture 70:30 of phosphate buffered saline solution and ethanol (PBS:EtOH). In each experiment 10 commercial drugs were also evaluated for assay validation. The graphic representation of experimental permeability *vs.* reported values of such well-known drugs gave a lineal correlation, *Pe* (exptl) = 0.69 *Pe* (bibl) + 6.61 (R^2 = 0.812). From this equation and taking into account the described limits for BBB permeation, we established that compounds with permeability values above 9.36 10^{-6} cm s^{-1} could penetrate into the CNS by passive diffusion (CNS+), whereas products with *Pe* below 7.98 10^{-6} cm s^{-1} could not enter (CNS–). Between these values, the CNS permeation was considered uncertain (CNS+/–). So, compound 3 (*Pe* =10.5 10^{-6} cm s^{-1}) would be able to cross BBB and reach its therapeutic targets.[48]

In order to better understand the overall properties and the drug-like characteristics of compounds 1-6, we carried out the calculation with Molinspiration software of the lipophilicity (expressed as the octanol/water partition coefficient and herein called logP), and the theoretical prediction of other ADME properties (molecular weight, TPSA, number of hydrogen donors and acceptors, and volume) (see Table 2).[49–51]

Table 2. Structural properties of the 3-aryl-6-methylcoumarin derivatives 1-6, and the reference compounds.

Comp.	logP[a]	MW [Da][b]	TPSA [Å^2][c]	nOH[d]	nOHNH[e]	Volume [Å^3][f]
1	4.07	281.27	76.04	5	0	239.89
2	4.10	281.27	76.04	5	0	239.89
3	4.12	281.27	76.04	5	0	239.89
4	3.60	251.28	56.23	3	2	227.84
5	3.21	251.28	56.23	3	2	227.84
6	3.24	251.28	56.23	3	2	227.84
Selegiline	2.64	187.29	3.24	1	0	202.64
Moclobemide	1.68	268.74	41.57	4	1	240.70

[a] LogP – expressed as the logarithm of octanol/water partition coefficient. [b] MW – Molecular weight [c] TPSA – Topological polar surface area. [d] Calculated octanol/water partition coefficient. [e] Number of hydrogen bond acceptors (nOH) and donors (nOHNH). [f] Molecular volume.

Reversibility experiments were performed to evaluate the type of inhibition of derivative 3, the most active compound in the series (Table 3). An effective dilution method was used,[52,53] and selegiline (irreversible inhibitor) and isatin (reversible inhibitor) were taken are standards.[54] Reversibility of the inhibition shown by compound 3 is even higher than that shown for isatin.

Table 3. Reversibility results of hMAO-B inhibition by derivative 3 and reference inhibitors.

Compound	Slope (AUF/t) [%][a]
3 (2.5 nM)	79.98 ± 5.33
Selegiline (20 nM)	8.51 ± 0.60
Isatin (35 μM)	64.71 ± 4.32

[a] Percentage values represent the mean ± SEM of three experiments (n = 3) relative to control; data show recovery of hMAO-B activity after dilution.

We also performed molecular docking simulations in the hMAO-B to detect the hypothetical binding mode for the 3-arylcoumarin derivatives 1-6 and explain their structure-activity relationship.[55–57] We used a similar protocol to previous studies.[58] We docked the compounds to the crystallized hMAO-B protein structure (PDB:2V60)[57] using Glide SP (Standard Precision mode).[56] Five poses for each compound were extracted from the

docking. The best pose was optimized using Prime MM–GBSA[56] along with the protein pocket (see Methods for a detailed description). To validate our protocol we calculated the root mean square deviation (RMSD) between the co–crystallized and the theoretical poses for the coumarins in 2V60 and 2V61.[57] RMSD values were 0.82 and 1.15 respectively.

As previous results for coumarin derivatives, the poses determined through molecular docking for the most of the studied compounds placed the benzopyrone ring with the carbonyl group oriented towards the bottom of the cavity. The methyl substituent at position 6 is oriented towards the FAD cofactor whereas the 3–aryl ring is placed in the hydrophobic entrance cavity. Compounds also established a hydrogen bond between the carbonyl oxygen and the residue Cys172. This described binding mode was found for compounds 2–6, showing the preference for this type of molecules to adopt the described conformation when interacting with the protein. However, docking for compound 1 (*ortho*–nitro) did not yield any poses as the one described. Figures 1 and 2 showed the proposed binding mode extracted from the docking calculations for compounds 1–6. The different binding mode proposed for the derivative 1 could be highly responsible for the loss of hMAO–B activity. Leu171 showed lower *van der Waals* interactions with compound 1, compared to compounds 2 and 3 with *meta* and *para* substituents (Figure 3a – supplementary material). Residue Coulomb contributions also showed a different profile between compound 1 and compounds 2 and 3.

For instance, Phe168 and Tyr435 exhibited poor Coulomb interaction energies with compound 1 whereas the residues Glu84 and Pro102 showed higher Coulomb interaction energies (Figure 3b – supplementary material).

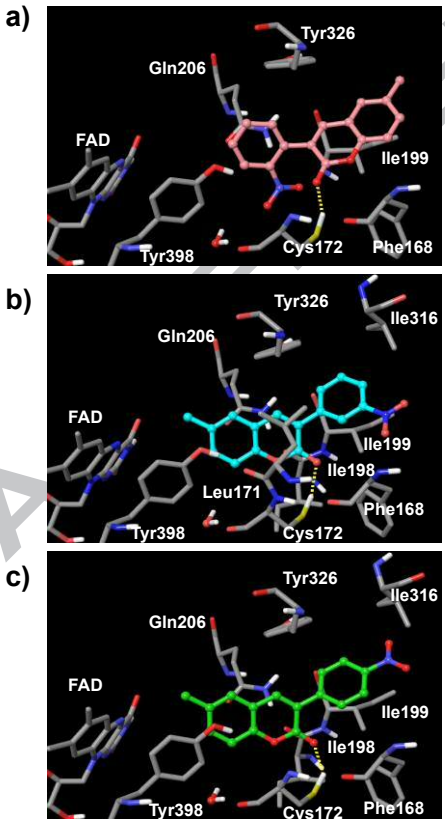

Figure 1. Hypothetical binding mode extracted from docking calculations for compound 1 (a), 2 (b) and 3(c). Hydrogen bonds between the compounds and the residue Cys172 are highlighted in yellow. Main residues interacting with the ligands are represented in tube.

Figure 2 shows the theoretical binding modes determined by compounds 4–6 along with the important residues interacting with the ligands. As an example, compound 5 establishes *van der Waals* interactions mainly with the residues Tyr326, Ile199, Leu171, Gln206, Cys172, Ile198, Phe168 and Ile316. Analysis of the binding mode showed important Coulomb contributions for residues Tyr326, Glu84 and Ile199. Compound 5 also showed a hydrogen bond between the carbonyl oxygen and the residue Cys172. Ligand conformation is also stabilized through different H–arene interactions between the ligand and the residues Leu171, Ile199 and Tyr326. However, in the comparison between compounds 4–6, compound 4 (*ortho*–amino) is slightly shifted towards the FAD cofactor (Figure 2d). Although the *ortho*–amino could establish a hydrogen bond with Tyr326, the pose determined for compound 4 would cause the disruption of some H–arene interactions, such as the interaction between the phenyl ring inTyr326 and the hydrogen at position 4 in the coumarin ring.

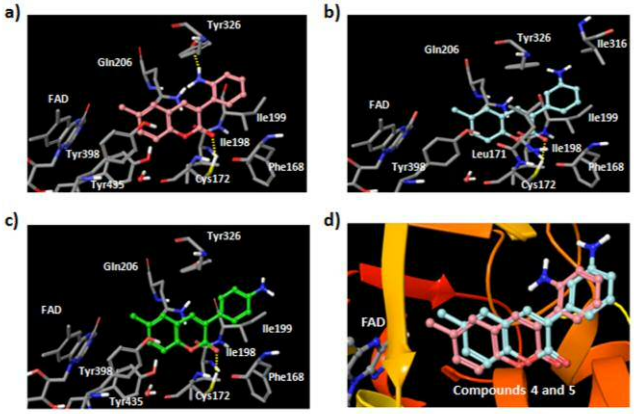

Figure 2. Hypothetical binding mode calculated with molecular docking for compound 4 (a), 5 (b) and 6 (c) along with the main residues (tube) that interact with the respective ligands. Hydrogen bonds with the residue Cys172 are highlighted in yellow. Compound 4 (a) also showed a hydrogen bond with the residue Tyr326. Panel d) shows the superposition of compounds 4 (pink color) and 5 (turquoise) inside the hMAO–B pocket. Compound 4 is slightly shifted towards the FAD cofactor.

Moreover, compounds 4–6 had some differences in the *van der Waals* and Coulomb energetic protein residue contributions. Compound 4 (*ortho*–amino) showed a drastic loss of *van der Waals* energy contribution with the residue Tyr326, compared to compounds 5 and 6 with *meta* and *para* amino substituents (Figure 4a – supplementary material). Moreover, lower *van der Waals* contributions were captured in residues Leu171 and Cys172 for compound 4. Coulomb interactions were also decreased for compound 4 in residues Glu84 and Cys172. However, Gln206 and Tyr326 exhibited more important electrostatic contributions in the interaction between compound 4 and the hMAO–B protein (Figure 4b – supplementary material). The amino substituent at *ortho* position could cause a small displacement of the coumarin nucleus with the consequent disruption of some stabilizer interactions with the protein and decreasing hMAO–B activity.

As represented in Table 1, most of the studied compounds showed a selective inhibitory activity against MAO–B in the nanomolar or micromolar range. The amino derivatives (4–6) proved to be slightly more selective against MAO–B than the nitro derivatives (1–3). The lowest IC_{50} values were obtained for

compounds 2, 3, 5 and 6 (*meta* and *para* derivative compounds), being the IC_{50} values in the low nanomolar range. In particular, compound 5 proved to be more than 9–fold more active and more than 12–fold more selective than selegiline, used as reference compound. Compounds 1 and 4, with IC_{50} values on the micromolar range, present on their structure a single substituent (NO_2 or NH_2, respectively) in *ortho* position of the phenyl at position 3. These results are consistent with those previously described for other 6–substituted–3–phenylcoumarins for which it was observed that the presence of substituents in *ortho* position produced a decrease in the MAO–B inhibitory activity (36). Compound 3 was the only exception observed for this series, presenting activity against the MAO–A isoenzyme (IC_{50} MAO–A = 4.18 μM).

From the data presented in Table 2, it is significant that almost all the derivatives described possess logP values compatible with those required to cross membranes. TPSA, described to be a predictive indicator of membrane penetration, was also found to be positive. In addition, it can be observed that no violations of Lipinski's rule (molecular weight, logP, number of hydrogen donors and acceptors) were found. As MAO inhibitors have to pass different membranes and reach the central nervous system, this information supports the potential of these derivatives. In addition, parallel artificial membrane permeation (PAMPA) assays were performed for compound 3, the most active derivative of the series. This compound proved to cross the BBB.

Compounds with *meta* and *para* substituents were well accommodated inside the hMAO–B protein pocket. The studied series showed a hypothetical binding mode that orientates the coumarin ring toward the FAD cofactor and the 3–aryl ring toward the hydrophobic entrance cavity. Carbonyl in the coumarin ring is placed in the bottom of the pocket and showed good availability to establish a hydrogen bond with the residue Cys172. However, the compounds with *ortho* substituents showed some differences according to docking simulations. Compound 1 did not yield any poses as the previously described showing a completely different binding mode that could condition the interaction with the hMAO–B. Moreover, although the pose shown by compound 4 is similar to the respective poses in compounds 5 and 6, the *ortho*–amino substituent established a hydrogen bond with the residue Tyr326 but at the same time led to a displacement of the coumarin nucleus towards the FAD and caused the disruption of some stabilizing interactions with Tyr326, Leu171 and Cys172. Binding conformations described in this article are in agreement with previous studies.[36,37,59,60]

Most of the studied compounds presenting structure of 3–arylcoumarin 1-6 behaved as potent and selective MAO–B inhibitors in vitro. These studies showed that *para* and *meta* derivatives of both series inhibited the activity of hMAO–B in the low nanomolar range, while *ortho* derivatives inhibited the activity of the same enzyme in the micromolar range. Compound 3 and 5 (IC_{50} = 2.1 and 2.2 nM, respectively) proved to be the most actives of the series, being 5 the most selective one (9–fold more active and 12–fold more selective than selegiline, the reference compound). In general, the amino derivatives proved to be more selective against MAO–B than the nitro derivatives. Molecular docking studies were performed to establish the nature of the interaction between the studied compounds and hMAO enzymes, leading to a rationalization of the experimental results for the synthesized series. Additionally, prediction of ADME–related physicochemical/structural parameters provided a preliminary indication of the great potential of this type of compounds to cross membranes and acting in the CNS. PAMPA assay of one of the best compounds experimentally corroborated these results. The global results encourage us to further explore the potential of this family of derivatives as potential lead candidates for the treatment of PD.

Acknowledgments

This work was partially supported by Spanish researchers personal funds and University of Santiago de Compostela. MJM thanks Fundação para a Ciência e Tecnologia for her postdoctoral grant (SFRH/BPD/95345/2013). SV thanks the Plan Galego de Investigación, Innovación e Crecemento 2011–2015 (I2C), European Social Fund (ESF) and Angeles Alvariño program from Xunta de Galicia (Spain). MIR–F thanks the Spanish Ministry of Economy and Competitiveness for financial support (SAF2012–31035).

References and notes

1. Trippier, P. C.; Labby, K. J.; Hawker, D. D.; Mataka, J. J.; Silverman, R. B. *J. Med. Chem.* 2013, *56*, 3121.
2. Meredith, G. E.; Totterdell, S.; Beales, M.; Meshul, C. K. *Exp. Neurol.* 2009, *219*, 334.
3. Zhu, Y.; Xiao, K.; Ma, L.; Xiong, B.; Fu, Y.; Yu, H.; Wang, W.; Wang, X.; Hu, D.; Peng, H.; Li, J.; Gong, Q.; Chai, Q.; Tang, X.; Zang, H.; Li, J.; Shen, J. *Bioorg. Med. Chem.* 2009, *17*, 1600.
4. Youdim, M. B. H. *Exp. Neurobiol.* 2010, *19*, 1.
5. Yahr, M. D.; Duvoisin, R. C.; Schear, M. J.; Barrett, R. E.; Hoehn, M. M. *Arch. Neurol.* 1969, *21*, 343.
6. Carlsson, A. *J. Neural Transm.* 2002, *109*, 777.
7. Abel, E. *Physiol. Behav.* 1995, *57*, 611.
8. Engberg, G.; Elebring, T.; Nissbrandt, H. *J. Pharmacol. Exp. Ther.* 1991, *259*, 841.
9. Scarpini, E.; Scheltens, P.; Feldman, H. *Lancet Neurol.* 2003, *2*, 539.
10. Bortolato, M.; Chen, K.; Shih, J. C. *Adv. Drug Deliv. Rev.* 2008, *60*, 1527.
11. Nagatsu, T. *Neurotoxicology* 2004, *25*, 11.
12. Venugopala, K. N.; Rashmi, V.; Odhav, B. *BioMed. Res. Inter.* 2013, *963248*, 1.
13. Murray, R. D. H. *Prog. Chem. Org. Nat. Prod.* 2002, *83*, 1.
14. Borges, F.; Roleira, F.; Milhazes, N.; Santana, L.; Uriarte, E. *Curr. Med. Chem.* 2005, *12*, 887.
15. Qian, L.–L.; Han, X.–E.; Han, H.; Chen, X.–Z.; Yuan, H.–H. *Guangzhou Huagong* 2013, *41*, 41.
16. Zheng, L.; Zhao, T.; Sun, L.–X. *Shizhen Guoyi Guoyao* 2013, *24*, 714.
17. Borges, F.; Roleira, F.; Milhazes, N.; Uriarte, E.; Santana, L. *Front. Med. Chem.* 2009, *4*, 23.
18. Bubols, G. B.; Vianna, D. R.; Medina–Remon, A.; von Poser, G.; Lamuela–Raventos, R. M.; Eifler–Lima, V. L.; Garcia, S. C. *Mini Rev. Med. Chem.* 2013, *13*, 318.
19. Xia, L.–X.; Wang, Y.–B.; Huang, W.–L.; Qian, H. *Zhongguo Xinyao Zazhi* 2013, *22*, 2392.
20. Kapoor, S. *Cytotechnology* 2013, *65*, 787.
21. Bansal, Y.; Sethi, P.; Bansal, G. *Med. Chem. Res.* 2013, *22*, 3049.
22. **O'Kennedy, R.** Biology, Applications and Mode of Action. Thornes, R.D. Ed., John Wiley and Sons, New York, USA, 1997.
23. Kontogiorgis, C.; Detsi, A.; Hadjipavlou–Litina, D. *Exp. Opin. Therap. Patents* 2012, *22*, 437.
24. Patil, P. O.; Bari, S. B.; Firke, S. D.; Deshmukh, P. K.; Donda, S. T.; Patil, D. A. *Bioor. Med. Chem.* 2013, *21*, 2434.
25. Anand, P.; Singh, B. *Arch. Pharmacal. Res.* 2013, *36*, 375.
26. Huang, L.; Su, T.; Li, X. *Curr. Top. Med. Chem.* 2013, *13*, 1864.

27. Di, L.; Kerns, E. H.; Fan, K.; McConnell, O. J.; Carter, G. T. *Eur. J. Med. Chem.* 2003, *38*, 223.
28. Anand, P.; Singh, B.; Singh, N. *Bioorg. Med. Chem.* 2012, *20*, 1175.
29. Helguera, A. M.; Perez-Machado, G.; Cordeiro, M. N. D. S.; Borges, F. *Mini Rev. Med. Chem.* 2012, *12*, 907.
30. Pisani, L.; Muncipinto, G.; Miscioscia, T. F.; Nicolotti, O.; Leonetti, F.; Catto, M.; Caccia, C.; Salvati, P.; Soto-Otero, R.; Mendez-Alvarez, E.; Passeleu, C.; Carotti, A. *J. Med. Chem.* 2009, *52*, 6685.
31. Secci, D.; Carradori, S.; Bolasco, A.; Chimenti, P.; Yáñez, M.; Ortuso, F.; Alcaro, S. *Eur. J. Med. Chem.* 2011, *46*, 4846.
32. Chimenti, F.; Secci, D.; Bolasco, A.; Chimenti, P.; Bizzarri, B.; Granese, A.; Carradori, S.; Yáñez, M.; Orallo, F.; Ortuso, F.; Alcaro, S. *J. Med. Chem.* 2009, *52*, 1935.
33. Matos, M. J.; Viña, D.; Vazquez-Rodriguez, S.; Uriarte, E.; Santana, L. *Curr. Top. Med. Chem.* 2012, *12*, 2210.
34. Santana, L.; González-Díaz, H.; Quezada, E.; Uriarte, E.; Yáñez, M.; Viña, D.; Orallo, F. *J. Med. Chem.* 2008, *51*, 6740.
35. Matos, M. J.; Vilar, S.; González-Franco, R. M.; Uriarte, E.; Santana, L.; Friedman, C.; Tatonetti, N. P.; Viña, D.; Fontenla, J. A. *Eur. J. Med. Chem.* 2013, *63*, 151.
36. Ferino, G.; Cadoni, E.; Matos, M. J.; Quezada, E.; Uriarte, E.; Santana, L.; Vilar, S.; Tatonetti, N. P.; Yañez, M.; Viña, D.; Picciau, C.; Serra, S.; Delogu, G. *Chem. Med. Chem.* 2013, *8*, 956.
37. Matos, M. J.; Terán, C.; Pérez-Castillo, Y.; Uriarte, E.; Santana, L.; Viña, D. *J. Med. Chem.* 2011, *54*, 7127.
38. Viña, D.; Matos, M. J.; Ferino, G.; Cadoni, E.; Laguna, R.; Borges, F.; Uriarte, E.; Santana, L. *Chem. Med. Chem.* 2012, *7*, 464.
39. Delogu, G.; Picciau, C.; Ferino, G.; Quezada, E.; Podda, G.; Uriarte, E.; Viña, D. *Eur. J. Med. Chem.* 2011, *46*, 1147.
40. Matos, M. J.; Gaspar, A.; Borges, F.; Uriarte, E.; Santana, L. *Org. Prep. Proc. Int.* 2012, *44*, 522.
41. Rao, D. V.; Sayigh, A. A. R.; Ulrich H. US 3644413 A 19720222, Chem. Abst., 77, 7318 (1972).
42. Chemistry – General methods: Starting materials and reagents were obtained from commercial suppliers and were used without further purification (Sigma–Aldrich). Melting points (mp) are uncorrected and were determined with a Reichert Kofler thermopan or in capillary tubes in a Büchi 510 apparatus. ^{1}H NMR (300 MHz) and ^{13}C NMR (75.4 MHz) spectra were recorded with a Bruker AMX spectrometer using DMSO-d_6 or $CDCl_3$ as solvent. Chemical shifts (δ) are expressed in ppm using TMS as an internal standard. Coupling constants (J) are expressed in Hz. Spin multiplicities are given as s (singlet), d (doublet), and m (multiplet). Mass spectrometry was carried out with a Hewlett–Packard-5972-MSD spectrometer. Elemental analyses were performed with a PerkinElmer 240B microanalyzer and are within 0.4% of calculated values in all cases. Flash chromatography (FC) was performed on silica gel (Merck 60, 230–400 mesh); analytical TLC was performed on pre-coated silica gel plates (Merck 60 F254). Organic solutions were dried over anhydrous Na_2SO_4. Concentration and evaporation of the solvent after reaction or extraction was carried out on a rotary evaporator (Büchi Rotavapor) operating at reduced pressure. The analytical results showed > 95% purity for all compounds.

General procedure for the synthesis of 6-methyl-3-nitrophenylcoumarins 1-3. To a dry 100-mL round-bottomed flask, the *ortho*-hydroxy-5-methylbenzaldehyde (42.5 mmol), the conveniently substituted nitrophenylacetic acid (42.5 mmol) and acetic anhydride (40.1 mL, 0.43 mol) were added. Then, sodium hydride (60% dispersion in mineral oil, 42.5 mmol) was added in small aliquots. After the dissolution of the reagents, precipitation process was observed (2-5 min). The reaction mixture was stirred for 20 h, and then water (7 mL) was added. After the addition of acetic acid (43 mL), the mixture was cooled to 4 °C for 4 h. The resulting precipitate was filtered and washed with cold glacial acetic acid. The acetic acid was then removed as an azeotrope upon addition of 250 mL toluene and evaporated to dryness. The process was repeated three times. The final residue was dried under vacuum and purified by FC (hexane/ethyl acetate 9:1) to give the products 1-3 as beige powders, in yields between 70-80%.

6-Methyl-3-**(2′**-nitrophenyl)coumarin (1) Yield: 70%. Mp: 95–96 °C. ^{1}H RMN (300 MHz; DMSO-d_6): δ= 2.39 (s, 3H, CH_3), 7.21-7.23 (m, 1H, H-**4'), 7.31**-7.37 (m, 2H, H-7, H-8), 7.39-7.48 (m, 3H, H-5, H-**5', H-6'), 7.63 (d,** *J* = 2.3 Hz, 1H, H-**3'), 7.75 (s,** 1H, H-4). ^{13}C RMN (75 MHz; DMSO-d_6): δ= 20.8, 116.4, 118.7, 123.7, 127.4, 127.8, 128.6, 130.1, 131.4, 132.9, 133.0, 134.2, 135.7, 142.5, 152.2, 160.9. DEPT (75 MHz; DMSO-d_6): δ= 20.8, 116.4, 127.4, 127.8, 130.1, 131.4, 132.9, 133.0, 142.5. MS (EI, 70 eV): *m/z* (%): 282 (14), 281 (M^+, 72), 178 (14), 136 (23), 90 (18). Anal. calcd. for $C_{16}H_{11}NO_4$: C, 68.32; H, 3.94. Found: C, 68.33; H, 3.96.

6-Methyl-3-**(3′**-nitrophenyl)coumarin (2) Yield: 74%. Mp: 96–97 °C. ^{1}H NMR (300 MHz; DMSO-d_6): δ= 2.37 (s, 3H, CH_3), 7.21 (d, *J* = 8.2 Hz, 2H, H-7, H-8), 7.50-7.56 (m, 2H, H-5, H-**5'), 7.87** (d, *J* = 6.5 Hz, 1H, H-**6'), 8.17 (s,** 1H, H-4), 8.28-8.37 (m, 2H, H-**2', H-4').** ^{13}C NMR (75 MHz; DMSO-d_6): δ= 20.6, 122.6, 123.9, 125.1, 127.9, 130.2, 131.4, 136.4, 136.6, 136.8, 137.2, 148.1, 149.3, 170.2, 190.6. DEPT (75 MHz; DMSO-d_6): δ= 20.6, 122.6, 123.9, 125.1, 130.2, 131.4, 136.6, 137.2, 190.6. MS (EI, 70 eV): *m/z* (%): 282 (8), 281 (M^+, 43), 253 (7), 235 (8), 178 (15), 163 (10), 136 (38), 90 (15). Anal. Elem. calcd. for $C_{16}H_{11}NO_4$: C, 68.32; H, 3.94. Found: C, 68.38; H, 3.99.

6-Methyl-3-**(4′**-nitrophenyl)coumarin (3). Yield: 80%. Mp: 100–101 °C.[20]

General procedure for the synthesis of 3-aminophenyl-6-methylcoumarins 4-6. The previously prepared 6-methyl-3-nitrophenylcoumarin (1, 2 or 3, 2.46 mmol) was dissolved in ethanol (5 mL) and a catalytic amount of Pd/C was added to the mixture. The solution was stirred, at room temperature, under a H_2 atmosphere, for 3 h. After completion of the reaction, the mixture was filtered to eliminate the catalyst. The obtained crude was then purified by flash chromatography (hexane/ethyl acetate 9:1) to give the desired coumarin 4-6 as white solids in yields between 92-97%.

3-**(2′**-Aminophenyl)-6-methyl-coumarin (4). Yield: 92%. Mp: 139–140 °C.[40]

3-**(3′**-Aminophenyl)-6-methyl-coumarin (5). Yield: 95%. Mp: 156–157 °C. ^{1}H NMR (300 MHz; $CDCl_3$): δ= 2.48 (s, 3H, CH_3), 3.98 (s, 2H, NH_2), 7.32-7.35 (m, 1H, H-**4'), 7.32**-7.40 (m, 2H, H-**5', H-6'), 7.55**-7.58 (m, 1H, H-7), 7.69-7.72 (m, 1H, H-8), 7.82 (s, 1H, H-**2'), 7.87**-7.91 (m, 1H, H-5), 7.92 (s, 1H, H-4). ^{13}C NMR (75 MHz; $CDCl_3$): δ= 24.9, 116.3, 125.4, 127.2, 127.8, 129.9, 130.0, 130.1, 131.4, 131.7, 132.9, 134.2, 134.4, 140.5, 151.8, 191.9. DEPT (75 MHz; $CDCl_3$): δ= 24.9, 116.3, 127.2, 127.8, 129.9, 131.4, 131.7, 132.9, 140.5. MS (EI, 70 eV): *m/z* (%): 252 (18), 251 (M^+, 90), 236 (90), 178 (18), 154 (19), 147 (21), 134 (58), 129 (25), 125 (18), 116 (20), 112 (37), 111 (29), 109 (17). Anal. calcd. for $C_{16}H_{13}NO_2$: C, 76.48; H, 5.21. Found: C, 76.39; H, 5.15.

3-**(4′**-Aminophenyl)-6-methyl-coumarin (6). Yield: 97%. Mp: 191–192 °C.[41]
43. Pharmacological assays – General methods: The tested compounds were dissolved in DMSO (Sigma–Aldrich, Alcobendas, Madrid, Spain) to prepare 10 mM stock solutions which were kept for storage at –20 °C. Percentage of DMSO used in the experiments was never higher than 1%. Selegiline, used as reference inhibitor, have been acquired from Sigma–Aldrich (Alcobendas, Madrid, Spain). Moclobemide has been kindly provided by Hoffman-La Roche Laboratories (Basel,

Switzerland). Human recombinant MAO isoforms, used in the experiments, was purchased from Sigma–Aldrich (Alcobendas, Madrid, Spain). Resorufin sodium salt, *p*–tyramine hydrochloride, sodium phosphate buffer, horseradish peroxidase and Amplex® Red reagent has been supplied in the assay kit of Amplex® Red MAO Molecular Probes (Molecular Probes, Inc., Eugene, Oregon, USA).

Determination of MAO isoforms enzymatic activity: Briefly, 0.1 mL of sodium phosphate buffer (0.05 M, pH 7.4) containing different concentrations of the test drugs (new compounds or reference inhibitors) in various concentrations and adequate amounts of recombinant hMAO–A or hMAO–B required and adjusted to obtain in our experimental conditions the same reaction velocity, i.e., to oxidize (in the control group) the same concentration of substrate: 165 pmol of *p*–tyramine/min (hMAO–A: 1.1 µg protein; specific activity: 150 nmol of *p*–tyramine oxidized to p–hydroxyphenylacetaldehyde/min/mg protein; hMAO–B: 7.5 µg protein; specific activity: 22 nmol of *p*–tyramine transformed/min/mg protein) were incubated for 15 min at 37 °C in a flat–black–bottom 96–well microtest plate, placed in the dark fluorimeter chamber. After this incubation period, the reaction was started by adding (final concentrations) 200 µM Amplex® Red reagent, 1 U/mL horseradish peroxidase and 1 mM *p*–tyramine. The production of H_2O_2 and, consequently, of resorufin was quantified at 37 °C in a multidetection microplate fluorescence reader (FLX800, Bio–Tek Instruments, Inc., Winooski, VT, USA) based on the fluorescence generated (excitation, 545 nm, emission, 590 nm) over a 15 min period, in which the fluorescence increased linearly.[43] Control experiments were carried out simultaneously by replacing the test drugs (new compounds and reference inhibitors) with appropriate dilutions of the vehicles. In addition, the possible capacity of the above test drugs to modify the fluorescence generated in the reaction mixture due to non–enzymatic inhibition (e.g., for directly reacting with Amplex® Red reagent) was determined by adding these drugs to solutions containing only the Amplex® Red reagent in a sodium phosphate buffer. To determine the kinetic parameters of hMAO–A and hMAO–B (K_m and V_{max}), the corresponding enzymatic activity of both isoforms was evaluated (under the experimental conditions described above) in the presence of a number (a wide range) of *p*–tyramine concentrations. The specific fluorescence emission (used to obtain the final results) was calculated after subtraction of the background activity, which was determined from wells containing all components except the hMAO isoforms, which were replaced by a sodium phosphate buffer solution. In our experimental conditions, this background activity was practically negligible. MAO activity of the test compounds and reference inhibitors is expressed as IC_{50}, ie the concentration of each drug required to produce a 50% decreased on control value activity isoforms MAO.

44. Yáñez, M.; Fraiz, N.; Cano, E.; Orallo, F. *Biochem. Biophys. Res. Commun.* 2006, *344*, 688.
45. Rodríguez–Franco, M. I.; Fernández–Bachiller, M. I.; Pérez, C.; Hernández–Ledesma, B.; Bartolomé, B. *J. Med. Chem.* 2006, *49*, 459.
46. Fernández–Bachiller, M. I.; Pérez, C.; Monjas, L.; Rademann, J.; Rodríguez–Franco, M. I. *J. Med. Chem.* 2012, *55*, 1303.
47. López–Iglesias, B.; Pérez, C.; Morales–García, J. A.; Alonso–Gil, S.; Pérez–Castillo, A.; Romero, A.; López, M. G.; Villarroya, M.; Conde, S.; Rodríguez–Franco, M. I. *J. Med. Chem.* 2014, *57*, 3773.

48. In vitro blood–brain barrier permeation assay: Prediction of the brain penetration was evaluated using a PAMPA–BBB assay, in a similar manner as previously described.[27,45-47] Pipetting was performed with a semi–automatic robot (CyBi®–SELMA) and UV reading with a microplate spectrophotometer (Multiskan Spectrum, Thermo Electron Co.). Commercial drugs, phosphate buffered saline solution at pH 7.4 (PBS), and dodecane were purchased from Sigma, Aldrich, Acros, and Fluka. Millex filter units (PVDF membrane, diameter 25 mm, pore size 0.45 µm) were acquired from Millipore. The porcine brain lipid (PBL) was obtained from Avanti Polar Lipids. The donor microplate was a 96–well filter plate (PVDF membrane, pore size 0.45 µm) and the acceptor microplate was an indented 96–well plate, both from Millipore. The acceptor 96 well microplate was filled with 200 µL of PBS:ethanol (70:30) and the filter surface of the donor microplate was impregnated with 4 mL of PBL in dodecane (20 mg mL^{-1}). Compounds were dissolved in PBS: ethanol (70:30) at 100 µg mL^{-1}, filtered through a Millex filter, and then added to the donor wells (200 µL). The donor filter plate was carefully put on the acceptor plate to form a sandwich, which was left undisturbed for 240 min at 25 °C. After incubation, the donor plate is carefully removed and the concentration of compounds in the acceptor wells was determined by UV–Vis spectroscopy. Every sample is analyzed at five wavelengths, in four wells and at least in three independent runs, and the results are given as the mean ± standard deviation. In each experiment, 10 quality control standards of known BBB permeability were included to validate the analysis set.
49. Theoretical evaluation of absorption, distribution, metabolism and excretion properties: The absorption, distribution, metabolism and excretion (ADME) properties of the studied compounds were calculated using the Molinspiration property programme. LogP was calculated using the methodology developed by Molinspiration as a sum of fragment–based contributions and correction factors (48). Topological polar surface area (TPSA) was calculated based on the methodology published by Ertl et al. as a sum of fragment contributions. Oxygenand nitrogen–centred polar fragments were considered (48). Polar surface area (PSA) has been shown to be a very good descriptor characterizing drug absorption, including intestinal absorption, bioavailability, Caco–2 permeability and blood–brain barrier penetration. The method for calculation of molecule volume developed at Molinspiration is based on group contributions. These have been obtained by fitting the sum of fragment contributions to 'real' threedimensional (3D) volume for a training set of about 12 000, mostly drug–like molecules. 3D molecular geometries for a training set were fully optimized by the semi–empirical AM1 method.
50. M cheminformatics, Bratislava, Slovak Republic, http://www.molinspiration.com/services/properties.html.

51. Lipinski, C. A.; Lombardo, F.; Dominy, B. W.; Feeney, P. J. *Adv. Drug Deliv. Rev.* 1997, *23*, 3.
52. Copeland, R. A. Evaluation of Enzyme Inhibitors in Drug Discovery, Wiley–Interscience, Hoboken, 2005.

53. Determination of inhibition mode To evaluate whether compounds 8, 14, and 15 are reversible or irreversible hMAO–B inhibitors, a dilution method was used.[52] A 100x concentration of the enzyme used in the above described experiments was incubated with a concentration of inhibitor equivalent to 10–fold its IC_{50} value. After 30 min, the mixture was diluted 100–fold into reaction buffer containing Amplex Red reagent, horseradish peroxidase, and p–tyramine, and the reaction was monitored for 15 min. Reversible inhibitors show linear progress with a slope equal to ~91% of the slope of the control sample, whereas irreversible inhibition reaches only ~9% of this slope. Control tests were carried out by pre–incubating and diluting the enzyme in the absence of inhibitor.

54. Gerlach, M.; Riederer, P.; Youdim, M. B. *Eur. J. Pharmacol.* 1992, *226*, 97.

55. Molecular docking calculations: We performed molecular docking simulations using the Schrödinger package.[56]

Ligand preparation: Our dataset is made out of the coumarin derivatives 1–6 and the co–crystallized coumarins in 2V60 and

2V61 (PDB code)[57] used to validate the docking protocol. We used LigPrep module[56] to generate possible protonation states at pH 7.0±2.0, possible tautomers, and optimized structures for all the ligands.

Protein preparation: We used the crystal structure of the hMAO–B (PDB:2V60) to run the docking simulations. In 2V60 the protein is bound to the coumarin derivative c17. We preprocessed the protein structure with the Protein Preparation Wizard.[56] In this step we assigned bond orders, added hydrogens, created disulfide bonds, filled possible missing side chains, added cap termini, deleted water molecules except the water that establishes a hydrogen bond with the co–crystallized coumarin derivative c17 and optimized the H–bond network, including reorientation of hydroxyl groups and optimization of the protonation state of some residues.

Receptor grid: As a previous step to docking, we generated a receptor grid centered in the coumarin derivative c17 with a length of 20 Å. The *van der Waals* scaling factor was 1.0 with 0.25 as a partial charge cut–off.

Molecular docking procedure: We performed molecular docking simulations in the hMAO–B using Glide Standard Precision level.[56] For each ligand, five poses were retained. The final pose selection was made based on the energy score E_{model}. Protein pocket and ligand poses were optimized using Prime MM–GBSA.[56]

56. Schrödinger package, Schrödinger, LLC, New York, NY, 2014. https://www.schrodinger.com.
57. Binda, C.; Wang, J.; Pisani, L.; Caccia, C.; Carotti, A.; Salvati, P.; Edmondson, D. E.; Mattevi, A. *J. Med. Chem.* 2007, *50*, 5848.
58. Matos, M. J.; Janeiro, P.; González–Franco, R. M.; Vilar, S.; Tatonetti, N. P.; Santana, L.; Uriarte, E.; Borges, F.; Fontenla, J. A.; Viña, D. *Fut. Med. Chem.* 2014, *6*, 371.
59. Matos, M. J.; Vilar, S.; García–Morales, V.; Tatonetti, N. P.; Uriarte, E.; Santana, L.; Viña, D. *Chem. Med. Chem.* 2014, *9*, 1488.
60. Ferino, G.; Vilar, S.; Matos, M.J.; Uriarte, E.; Cadoni E. *Curr. Top. Med. Chem.* 2012, *12*, 2145.